Dominant phonon polarization conversion across dimensionally mismatched interfaces: Carbon-nanotube–graphene junction

Jingjing Shi,[1] Jonghoon Lee,[2,3] Yalin Dong,[1,4] Ajit Roy,[2] Timothy S. Fisher,[5] and Xiulin Ruan[1,*]

[1]*School of Mechanical Engineering and Birck Nanotechnology Center, Purdue University, West Lafayette, Indiana 47907, USA*

[2]*Materials and Manufacturing Directorate, Air Force Research Laboratory, Wright-Patterson Air Force Base, Ohio 45433, USA*

[3]*Universal Technology Corporation, 1270 North Fairfield Road, Dayton, Ohio 45432, USA*

[4]*Department of Mechanical Engineering, The University of Akron, Akron, Ohio 44325, USA*

[5]*Department of Mechanical and Aerospace Engineering & California NanoSystems Institute, University of California Los Angeles, Los Angeles, California 90095, USA*

(Received 3 April 2017; revised manuscript received 19 March 2018; published 30 April 2018)

Dimensionally mismatched interfaces are emerging for thermal management applications, but thermal transport physics remains poorly understood. Here we consider the carbon-nanotube–graphene junction, which is a dimensionally mismatched interface between one- and two-dimensional materials and is the building block for carbon-nanotube (CNT)–graphene three-dimensional networks. We predict the transmission function of individual phonon modes using the wave packet method; surprisingly, most incident phonon modes show predominantly polarization conversion behavior. For instance, longitudinal acoustic (LA) polarizations incident from CNTs transmit mainly into flexural transverse (ZA) polarizations in graphene. The frequency stays the same as the incident mode, indicating elastic transmission. Polarization conversion is more significant as the phonon wavelength increases. We attribute such unique phonon polarization conversion behavior to the dimensional mismatch across the interface, and it opens significantly new phonon transport channels as compared to existing theories where polarization conversion is neglected.

DOI: 10.1103/PhysRevB.97.134309

I. INTRODUCTION

Thermal interfacial resistance is a critical issue for thermal management of modern electronic devices. Planar interfaces have been extensively studied, and theories such as the acoustic mismatch model (AMM) [1] have been successfully developed to predict mode-resolved phonon transport. On the other hand, dimensionally mismatched nonplanar interfaces, such as one-dimensional–two-dimensional (1D-2D) [2–6], one-dimensional–three-dimensional (1D-3D) [7–11], and 2D-3D [12–14] interfaces, are emerging for many applications, but existing theories may not describe their thermal interfacial transport correctly due to new physics introduced by the dimensional mismatch. An attempt of the modified acoustic mismatch model has been made at 1D-3D interface [11], but has not been compared to simulation or experimental results. As an example of a dimensionally mismatched interface, the current work will consider the carbon-nanotube (CNT)–graphene junction, which is an interface between 1D and 2D materials and is the building block for CNT–graphene 3D networks recently proposed and synthesized [2–6]. Although CNTs [13,15,16] and graphene [17–21] have very high thermal conductivity, they both suffer from anisotropy in thermal transport. The thermal conductivity of graphene stacks or graphite in the cross-plane direction is two or more orders of magnitude lower than that of the in-plane direction [22]. CNT bundles also show similar behavior in the radial direction [23]. Therefore, the above-mentioned 3D CNT-graphene network was proposed to achieve high thermal conductivity in all directions. Our previous nonequilibrium molecular dynamics (NEMD) simulations indicate that the thermal resistance in the network primarily comes from CNT–graphene junctions [6]. However, the NEMD method gives only an overall thermal boundary resistance without any physical insights associated with the unique dimensional mismatch nature. The CNT-graphene junctions have been synthesized in the experiment [5], but the interfacial thermal transport has not been measured yet. Hence, it is a timely task to understand interfacial thermal transport physics across the 1D-2D junction and assess the validity of the existing theoretical models. The results will lend useful insights for 1D-3D and 2D-3D interfaces as well.

In this work, we report the modal phonon transmission process at CNT-graphene junctions using the wave packet method [4,9,24,25], which is an accurate spectral phonon transmission simulation method. The junction is between a (6,6) CNT and graphene sheet with sp^2 covalent bonds. The schematic of the simulated structure is shown in Fig. 1(a). We find intriguing phonon polarization conversion behavior during the transmission process for all incident modes from CNT, i.e., they partially convert to different phonon polarizations in graphene after the transmission. Such surprising behavior cannot be captured by the conventional mismatch models.

II. METHODS

The molecular dynamics (MD) phonon wave packet method is implemented with the LAMMPS package. We use the classical

*ruan@purdue.edu

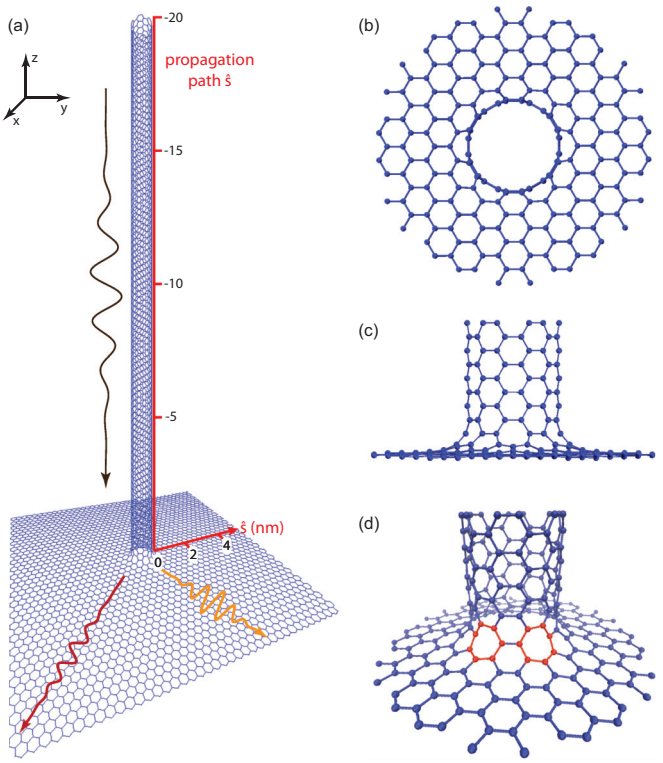

FIG. 1. (a) Schematic of the pillared graphene structure used in this work. (b) Top view and (c) front view of the detailed junction structure. (d) Detailed junction structure with perspective, where the heptagon defects are highlighted with red.

molecular dynamics since only a single mode wave packet is launched in each simulation and quantum factors are not important. The detailed structure of the CNT–graphene junction is shown in Figs. 1(b) to 1(d). The interactions between carbon atoms in lattice dynamics calculations and MD simulations are based on the polymer consistent force field (PCFF) [26,27]. The phonon dispersion relation and mode eigenvectors of (6,6) CNT are first calculated. To create a wave packet for a specific phonon mode, the initial displacement from equilibrium and velocity of the ith base atom in the nth unit cell along the α direction are [4]

$$u^{\gamma}_{ni\alpha} = \frac{A}{\sqrt{M}} \sum_{q} \exp\left[-\frac{(q-q_0)^2}{2\sigma^2}\right] \times \varepsilon^{\gamma}_{i\alpha}(q) \exp\left[iq(z_n - z_0)\right], \quad (1)$$

$$v^{\gamma}_{ni\alpha} = \frac{A}{\sqrt{M}} \sum_{q} -i2\pi v^{\gamma}(q) \exp\left[-\frac{(q-q_0)^2}{2\sigma^2}\right] \times \varepsilon^{\gamma}_{i\alpha}(q) \exp[iq(z_n - z_0)], \quad (2)$$

where A is the amplitude, M is the carbon atom mass, q_0 is the wave number of the packet, z_0 and z_n are the positions of the packet center and the nth unit cell in the CNT along the propagation path $\hat{s}$, and ε is the eigenvector of the phonon with wave number q and polarization γ. As shown in Fig. 1(a), the phonon wave packet is activated from the CNT with a specific polarization γ and propagates towards the graphene sheet.

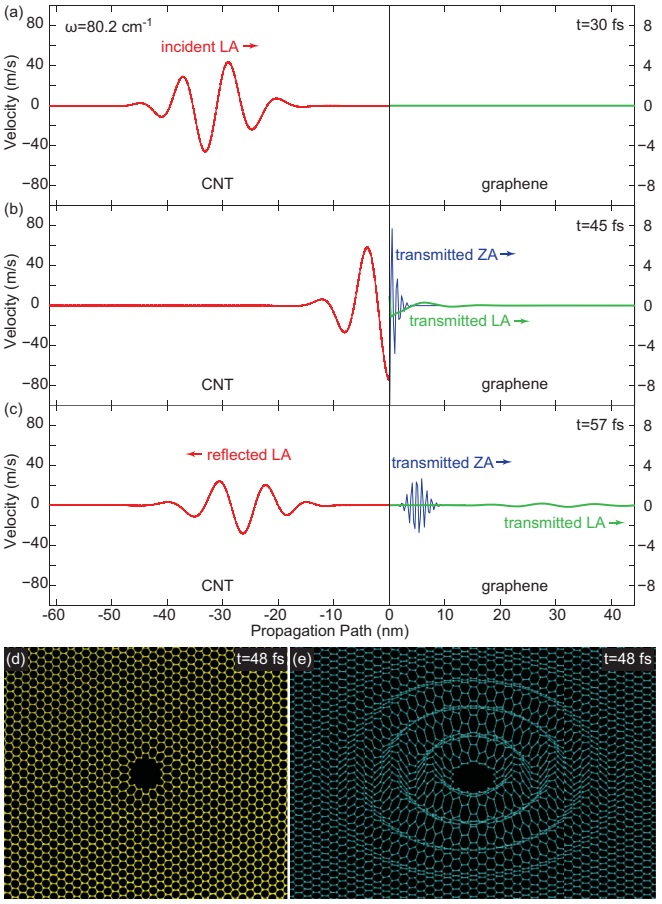

FIG. 2. Typical wave packet propagation process for an incident LA mode from CNT. Atom velocity (the left axis is the scale of atom velocity in CNT, the right axis is the scale of atom velocity in graphene) (a) plot before the wave packet reaches the interface, (b) when the wave packet just reaches the interface, and (c) after transmission. (d) In-plane displacements (amplified by 600 times) of graphenen atoms. (e) Out-of-plane displacements (amplified by 600 times) of graphene atoms.

After the wave packet reaches the junction, the transmitted part continues to propagate into graphene, and the reflected part propagates back to the CNT as shown in Figs. 2(a) to 2(c). Monitoring the amount of energy transmitted or reflected at the junction enables the calculation of the energy transmission coefficient of the specific phonon mode. For the reflected part, the wave number can be calculated using the Fourier transform of atom velocity at different positions, and the frequency can be calculated using the Fourier transform of atom velocity at different time. For the transmitted part in graphene, the energy propagates in the radial direction, so the velocity of an array of atoms along the radius scaled by the square root of radius $v \cdot \sqrt{r}$ is used in the Fourier transform. According to Parseval's theorem, the energy of each transmitted wave packet with a specific wave number can be calculated by the integral over the square of the amplitude of Fourier transform result. Because of the anisotropy in graphene, the transmission coefficients are different along different radial directions. Hence, both the zigzag and armchair directions are used in the Fourier transform and are averaged to determine the

overall transmission coefficient. The details of the calculation of transmission coefficient can be found in the Supplemental Material [28]. We confirm energy conservation by checking that the sum of the transmitted and reflected energies equals the incident energy.

III. RESULTS AND DISCUSSION

In the molecular dynamics simulation, we launch wave packets of longitudinal acoustic (LA), transverse acoustic (TA), twisting (TW), and radial breathing (RB) polarizations with different wave numbers in the CNT because these acoustic polarizations and high group velocity polarizations are more important in thermal transport. These phonon modes are launched one at a time to predict mode-resolved transmission behavior. We find that the reflected phonon frequency, wave number, and polarization remain the same as the incident mode, indicating an elastic reflection process. This can also be seen from Fig. 2(b): the superposition of incident and reflected waves in the CNT near the interface has exactly the same wavelength as the incident wave packet.

However, the transmission shows surprising polarization conversion behavior, as shown in Fig. 2. The incident LA phonon polarization from CNT transmits into both LA and ZA polarizations in graphene, and the amplitude of the ZA polarization is much larger than that of the LA polarization, as is shown clearly in Figs. 2(b) and 2(c). A video of phonon propagation can be found in the Supplemental Material as video A [28]. After the Fourier transform of modified atom velocities $v \cdot \sqrt{r}$ at different positions in graphene, two transmitted modes with their respective wave numbers are clearly seen as two peaks in graphene k-space as shown in Fig. 3(b). Since the phonon dispersion relation of graphene has been obtained, the polarizations can be confirmed according to their frequencies and wave numbers. Using polarization and wave numbers, we can identify these modes as two dots on LA and ZA branches of the graphene phonon dispersion relation respectively, as shown in Fig. 3(d). Despite polarization conversion, the frequency of these transmitted modes is the same as the incident LA mode in the CNT, as shown in Figs. 3(b) and 3(d), indicating that the transmission process is also elastic without anharmonic phonon scattering. Hence, the transmitted LA and ZA wave packets in graphene have different wave numbers, wavelengths, and group velocities. Figure 2(c) clearly shows that the LA and ZA wave packets propagate at different speeds. Figures 2(d) and 2(e) show the in-plane and out-of-plane atomic displacements in graphene, respectively, for an incident LA wave packet. Because the graphene LA polarization only has in-plane displacement and velocity, while the ZA polarization only has out-of-plane displacement and velocity, the decomposition in Figs. 2(d) and 2(e) indicates that both LA and ZA modes are indeed induced in graphene. Inelastic mode conversion behaviors have been observed at silicon germanium interface with roughness [25] due to the anharmonic phonon scattering at the rough interface, and the effect is very small. Elastic phonon polarization conversions [29,30] have been observed in 3D superlattice or pure crystal for oblique incident phonon at high frequency. However, our polarization conversion at a single interface between low-dimensional materials due to dimensional mismatch is very different from these conversions. The polarization conversion we observed at the CNT–graphene junction is elastic and dominates the transmission from low frequency to high frequency.

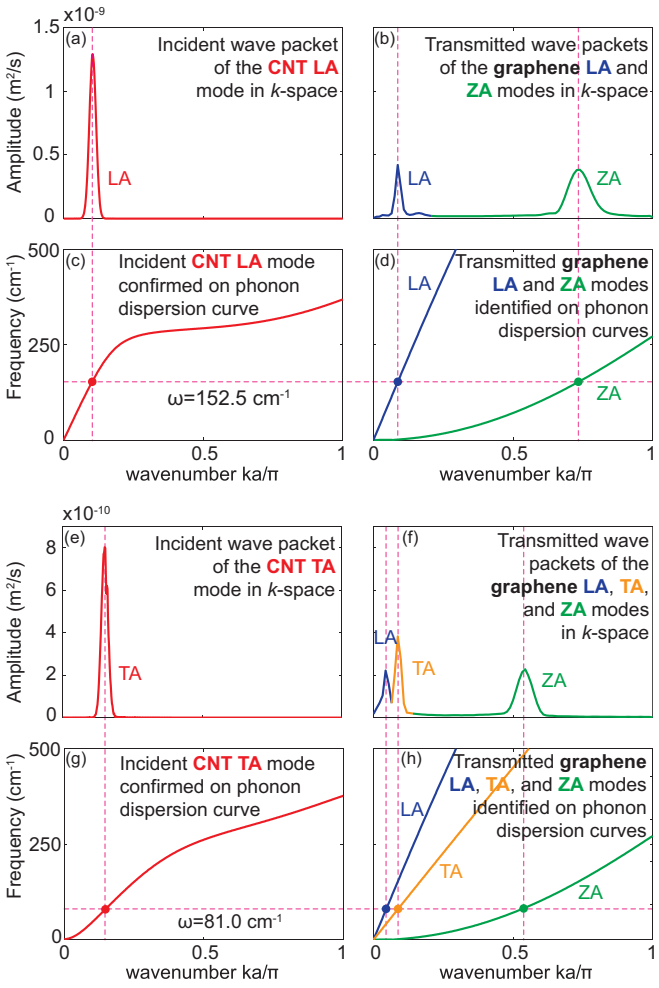

FIG. 3. (a) An incident CNT LA wave packet and (b) its transmitted graphene LA and ZA wave packets in k space, and (c) the corresponding identified modes on CNT LA branch and (d) graphene LA and ZA branches, respectively. (e) An incident CNT TA wave packet and (f) its transmitted graphene LA, TA, and ZA wave packets in k space, and (g) the corresponding identified modes on CNT TA branch and (h) graphene LA, TA, and ZA branches, respectively.

Like the incident LA polarization from CNT, the incident TA and other polarizations also exhibit polarization conversion behavior after transmission. For the incident TA wave packet shown in Fig. 3(e), the transmission process is more complicated since the phonon eigenvector of the CNT TA polarization not only has axial and radial components like the LA, but also tangential component. The transmitted phonons into graphene are LA, TA, and ZA polarizations, as shown as three peaks in as shown in Fig. 3(f). The transmission process is similar to the incident LA polarization, where the frequency does not change, and transmitted modes can be identified as three dots on the LA, TA, and ZA branches of the graphene dispersion relation, as shown in Figs. 3(g) and 3(h). For the incident TW polarization from the CNT, the transmitted polarizations are TA and ZA because the motion of the TW polarization in the CNT is

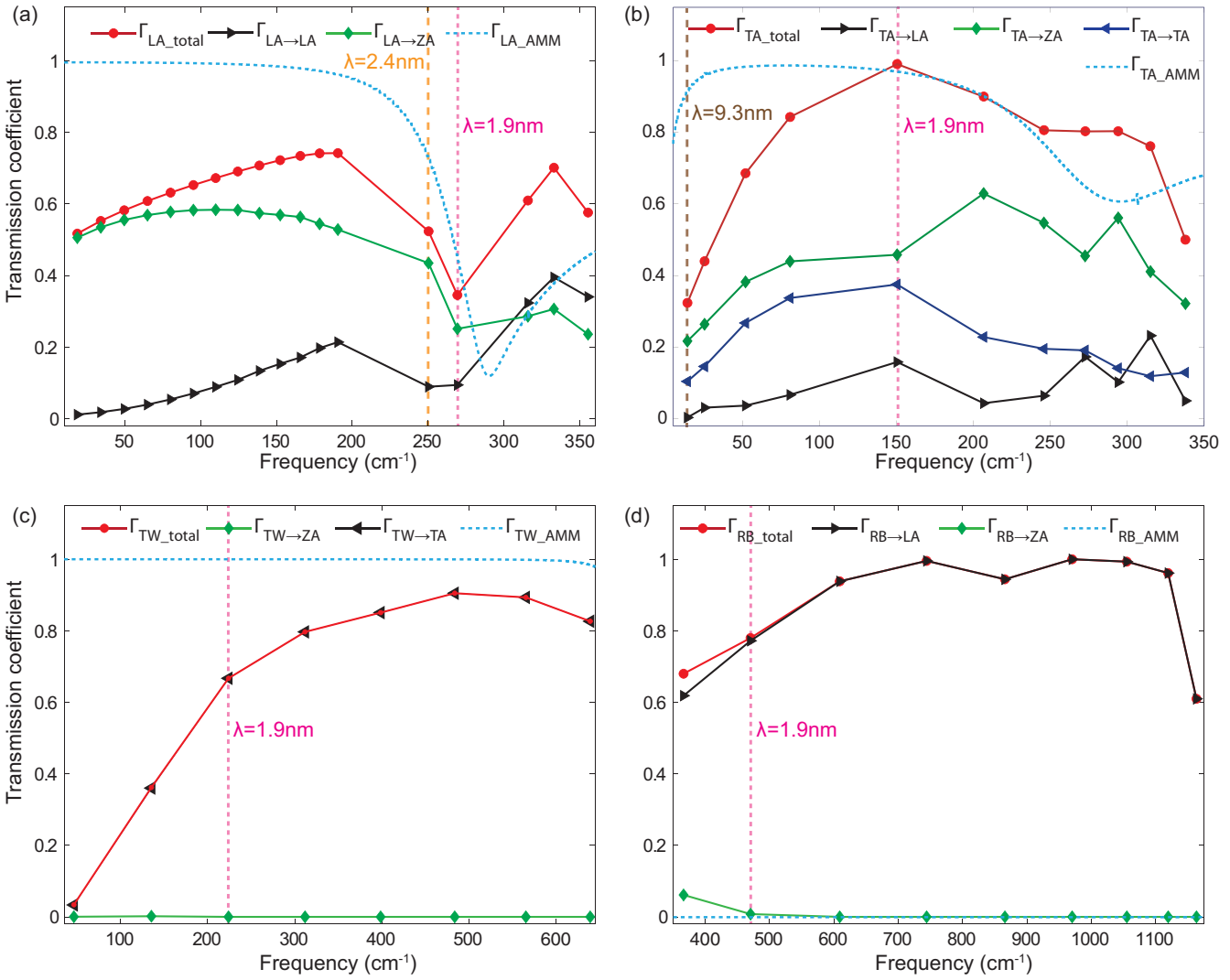

FIG. 4. Transmission coefficients of incident (a) LA, (b) TA, (c) TW, and (d) RB polarizations.

along the tangential direction, which has similar displacement as the TA polarization in graphene (in-plane transverse). For the incident RB polarization, the transmitted polarizations are LA and ZA just like the incident CNT LA polarization because the axial and radial displacements of the CNT RB polarization are similar to the displacement of the CNT LA polarization. A video of atomic vibrations of different polarizations (LA, TA, TW, and RB) in the CNT can be found in the Supplemental Material as video B [28].

We attribute the unique polarization conversion behavior across the CNT-graphene to the special dimensionally mismatched structure and defects of the system. During the transmission from 1D CNT to 2D graphene, the propagation direction of phonons must change 90 degrees as shown in Fig. 1(c), and there are six heptagonal defects as shown in Fig. 1(d). For a given incident mode such as an LA mode in CNT, some of the transmitted energy preserves the polarization without conversion, i.e., LA to LA, while the remaining transmitted energy preserves the direction of atomic vibrations or involve in some more complex process and will change polarization, i.e., LA to ZA. We suspect that the polarization conversion behavior is related to the wavelength of the incident phonon wave; hence we investigate the transmission coefficient as a function of the phonon frequency, which is directly related to the wavelength.

In Fig. 4, we show the transmission coefficient of each individual incident phonon polarization, as well as the breakdown into different transmitted polarizations in graphene. The transmission coefficient Γ_{X_total} is defined as the transmitted energy into the graphene over the incident energy from CNT in the polarization X. The notation $\Gamma_{X\to Y}$ means the breakdown transmission coefficient into a specific graphene polarization Y from incident CNT polarization X. It is found that the polarization conversion is more significant for long incident wavelengths (small wave number). Figure 4(a) shows that for long wavelength incident LA polarization, the transmission into the ZA polarization dominates over that into the LA polarization. It can be explained in this way. Long wavelength means the neighboring atoms in CNT vibrate almost in phase. When the motion propagates through the junction, the direction of atomic displacement (mainly along the axial direction in CNT) is largely preserved since the wavelength is much larger than the radius of curvature of the junction (about 0.5 nm). Therefore, most of the transmitted vibration becomes the ZA

polarization. As the wavelength decreases, the neighboring atoms start to vibrate out of phase, and the wavelength becomes closer to the junction radius of curvature. Hence, the atomic motion originally along the axial direction in CNT can better adapt to the junction and induce more in-plane (xy plane) motion in graphene. A video to describe the phenomenon is provided in the Supplemental Material as video C [28]. Therefore, $\Gamma_{LA\to LA}$ increases with decreasing wavelength.

For the incident TA polarization as shown in Fig. 4(b), the transmission into the ZA polarization dominates over that into other polarizations (LA and TA). In the long wavelength range, the polarization conversion is also more important like the incident LA polarization. About 67% of the total transmitted energy is into the ZA polarization when the frequency is about 14 cm^{-1} (wavelength λ is around 9.3 nm), and about 46% of the total transmitted energy is into the ZA polarization when the frequency is about 151 cm^{-1} (wavelength λ is around 1.9 nm). Although polarization conversion behavior dominates the transmission, the transmission process of the incident TA polarization is very different from the LA polarization. The direction of atomic displacement of the incident TA is mainly along the radial and tangential directions in CNT, while that of the transmitted ZA is along the axial direction in CNT. Hence the polarization conversion behavior like TA to ZA is a complex phenomenon that cannot be described by one simple or intuitive rule that the dominant transmitted mode will preserve the atomic vibration direction. The polarization conversion from TA to ZA might relate to the complexity of CNT TA polarization and the similarity shared by phonon dispersion relations of these two branches. For the incident TW polarization (in-plane transverse), polarization conversion to ZA (out-of-plane transverse) is more significant at long wavelength as shown in Fig. 4(c). For the incident RB polarization (atoms mainly vibrate perpendicularly to energy propagation direction), polarization conversion to LA (atoms mainly vibrate along energy propagation direction) dominates the transmission as shown in Fig. 4(d). For the incident TW and RB polarizations, most transmissions preserve the atomic vibration direction.

Next we compare our simulation results to those from analytical models. Acoustic mismatch and diffuse mismatch models are commonly used for interfacial thermal transport. Here the acoustic mismatch model (AMM) is used since the sp^2 covalent bond is very strong and the interface is smooth. The transmission coefficient from AMM, Γ_{X_AMM}, is generally higher than the total transmission coefficient Γ_{X_total} from our wave packet method especially at long wavelengths, as shown in Fig. 4. The lower transmission from the wave packet simulation can be attributed to the nonplanar interface and defects (six heptagons at the interface as shown in Fig. 1). The difference between Γ_{X_AMM} and Γ_{X_total} at longer incident wavelength is more significant because the junction appears to be more abrupt for longer wavelength wave packets, while it is smoother for shorter wavelength packet when the wavelength is comparable to or smaller than the junction radius of curvature.

On the other hand, from Figs. 4(a) and 4(b), Γ_{X_total} is sometimes higher than Γ_{X_AMM} at certain short wavelengths (incident wavelength $\lambda < 1.9$ nm as shown by pink dashed line). In fact, these higher Γ_{X_total} are due to polarization conversion. AMM assumes that one polarization transmits into the same polarization. However, at the CNT–graphene junction, the existence of polarization conversion provides an additional channel to transfer heat, such that Γ_{X_total} can be larger than Γ_{X_AMM}. If we compare Γ_{LA_AMM} to $\Gamma_{LA\to LA}$ alone for the incident LA polarization, we can see that Γ_{LA_AMM} is indeed generally higher than $\Gamma_{LA\to LA}$ especially at long wavelength. The difference between Γ_{LA_AMM} and Γ_{LA_total} when $\lambda < 1.9$ nm is completely from polarization conversion $\Gamma_{LA\to ZA}$. Interestingly, when compared to the transmission coefficient from one polarization to the same one, AMM can still capture some features of transmission. For example, $\Gamma_{LA\to LA}$ shows a minimum at around 250 cm^{-1} (wavelength $\lambda = 2.4$ nm), and Γ_{LA_AMM} also shows a minimum at around 290 cm^{-1}. This minimum from AMM is due to the large mismatch in the group velocities of CNT and graphene, which can be found from the phonon dispersion relation FIG. S2 in the Supplemental Material [28].

TABLE I. The CNT–graphene interface thermal conductance results predicted from Landauer approach with transmission functions from wave packet (WP) method (without and with polarization conversion) and AMM of incident LA, TA, TW, and RB branches.

Polarization	$G_{WPw/o}$ (W/m^2K)	$G_{WPw/}$ (W/m^2K)	G_{AMM} (W/m^2K)
LA	5.02×10^7	2.14×10^8	2.22×10^8
TA	1.36×10^8	4.35×10^8	6.18×10^8
TW	4.64×10^8	4.65×10^8	1.17×10^{10}
RB	0	9.92×10^8	0

To understand how the polarization conversion affects thermal conductance, we applied the Landauer formula [31] with the above transmission functions from wave packet and AMM, respectively, to calculate thermal conductance at the pillared graphene interface, and compare the results. The Landauer formula is

$$q = \frac{1}{2\pi}\int_0^{+\infty} \hbar\omega[M_1(\omega)\tau_{1\to2}(\omega)f(T_1) - M_2(\omega)\tau_{2\to1}(\omega)f(T_2)]d\omega, \quad (3)$$

where $M(\omega)$ is the number of modes at a given frequency ω, $\tau(\omega)$ is the transmission coefficient at the interface from one material to the other, and $f(T)$ is the Bose-Einstein distribution function at temperature T. The equivalent equilibrium temperature correction [32] is used since the transmission coefficients are high at the CNT–graphene junction. As shown clearly in Table I, for the incident LA polarization, the polarization conversion increases the conductance from 5.02×10^7 W/m^2K to 2.14×10^8 W/m^2K. The contribution of polarization conversion is 76.5% of the total conductance. For the incident TA polarization as shown in Table I, the contribution of polarization conversion, which is 68.7% of the total also dominates. Interestingly, for the incident RB polarization, since there is no corresponding polarization in graphene, the conductance without polarization conversion is 0, and the contribution of polarization conversion is 100%. When compared to the conductance results from AMM transmission coefficients, G_{LA_WP} is comparable to G_{LA_AMM} because Γ_{LA_total} is generally smaller than Γ_{LA_AMM}, but larger than Γ_{LA_AMM} at high frequency. For TA and TW branches,

G_{WP} is smaller than G_{AMM} since the transmission Γ_{total} is generally smaller than Γ_{AMM}. For the RB branch, as we mentioned above, since there is no corresponding polarization in graphene, G_{RB_AMM} is 0, and G_{RB_WP} is much larger than it. From the interface thermal conductance calculation, it shows that polarization conversion dominates most incident phonon polarizations, and the interface conductance with transmission from wave packet G_{WP} can be smaller than G_{AMM} when the transmission is smaller, and can also exceed G_{AMM} because the former includes while the latter neglects polarization conversion. Therefore, the unique junction between 1D CNT and 2D graphene on one hand tends to reduce the transmission and interface conductance due to the defects and dimensional mismatch, while on the other hand tends to enhance the transmission and conductance due to polarization conversion. The overall effect depends on which mechanism dominates.

IV. SUMMARY AND CONCLUSION

To summarize, we predict the transmission function of individual phonon mode using the wave packet method at CNT–graphene junction, which is a dimensionally mismatched interface between 1D and 2D materials. Intriguing phonon polarization conversion behavior is observed for most incident phonon modes. Polarization conversion is found to dominate the transmission and is more significant at larger phonon wavelength. We attribute such unique phonon polarization conversion behavior to the dimensional mismatch and defects across the CNT–graphene interface. The polarization conversion is a complicated phenomenon related to interface atomic structure, phonon polarization, direction of atomic displacement, and phonon dispersion relations. As such, the transmission functions and interfacial conductance at the junction cannot be explained by the conventional acoustic mismatch models. The dimensionally mismatched interface on one hand tends to reduce the transmission and conductance due to defects and the change of phonon propagation direction, while on the other hand tends to enhance the transmission and conductance due to the new phonon transport channel introduced by polarization conversion.

ACKNOWLEDGMENT

The authors would like to acknowledge the support by the Air Force Office of Scientific Research (AFOSR) MURI Grant No. (FA9550-12-1-0037).

[1] E. T. Swartz and R. O. Pohl, Rev. Mod. Phys. **61**, 605 (1989).
[2] G. K. Dimitrakakis, E. Tylianakis, and G. E. Froudakis, Nano Lett. **8**, 3166 (2008).
[3] V. Varshney, A. K. Roy, G. Froudakis, and B. L. Farmer, Nanoscale **3**, 3679 (2011).
[4] J. Lee, V. Varshney, J. S. Brown, A. K. Roy, and B. L. Farmer, Appl. Phys. Lett. **100**, 183111 (2012).
[5] Y. Xue, Y. Ding, J. Niu, Z. Xia, A. Roy, H. Chen, J. Qu, Z. L. Wang, and L. Dai, Sci. Adv. **1**, e1400198 (2015).
[6] J. Shi, Y. Dong, T. Fisher, and X. Ruan, J. Appl. Phys. **118**, 044302 (2015).
[7] I. Duchemin and D. Donadio, Phys. Rev. B **84**, 115423 (2011).
[8] B. A. Cola, J. Xu, C. Cheng, X. Xu, T. S. Fisher, and H. Hu, J. Appl. Phys. **101**, 054313 (2007).
[9] M. Hu, P. Keblinski, J. S. Wang, and N. Raravikar, J. Appl. Phys. **104**, 083503 (2008).
[10] Y. Wang, X. Ruan, and A. K. Roy, Phys. Rev. B **85**, 205311 (2012).
[11] R. Prasher, T. Tong, and A. Majumdar, J. Appl. Phys. **102**, 104312 (2007).
[12] J. H. Seol, I. Jo, A. L. Moore, L. Lindsay, Z. H. Aitken, M. T. Pettes, X. Li, Z. Yao, R. Huang, D. Broido, N. Mingo, R. S. Ruoff, and L. Shi, Science **328**, 213 (2010).
[13] B. Qiu, Y. Wang, Q. Zhao, and X. Ruan, Appl. Phys. Lett. **100**, 233105 (2012).
[14] Z. Wang, T. Feng, and X. Ruan, J. Appl. Phys. **117**, 084317 (2015).
[15] J. Shiomi and S. Maruyama, Phys. Rev. B **73**, 205420 (2006).
[16] L. Lindsay, D. A. Broido, and N. Mingo, Phys. Rev. B **82**, 161402(R) (2010).
[17] A. A. Balandin, S. Ghosh, W. Bao, I. Calizo, D. Teweldebrhan, F. Miao, and C. N. Lau, Nano Lett. **8**, 902 (2008).
[18] S. Ghosh, I. Calizo, D. Teweldebrhan, E. P. Pokatilov, D. L. Nika, A. A. Balandin, W. Bao, F. Miao, and C. N. Lau, Appl. Phys. Lett. **92**, 151911 (2008).
[19] L. Lindsay, D. A. Broido, and N. Mingo, Phys. Rev. B **82**, 115427 (2010).
[20] J. Hu, X. Ruan, and Y. P. Chen, Nano Lett. **9**, 2730 (2009).
[21] Y. Wang, B. Qiu, and X. Ruan, Appl. Phys. Lett. **101**, 13101 (2012).
[22] A. A. Balandin, Nat. Mater. **10**, 569 (2011).
[23] J. Che, T. Cagin, and W. Goddard, Nanotechnology **11**, 65 (2000).
[24] Z. T. Tian, B. E. White, and Y. Sun, Appl. Phys. Lett. **96**, 263113 (2010).
[25] L. Sun and J. Y. Murthy, J. Heat Transfer **132**, 102403 (2010).
[26] H. Sun, S. J. Mumby, J. R. Maple, and A. T. Hagler, J. Am. Chem. Soc. **116**, 2978 (1994).
[27] H. Sun, J. Phys. Chem. B **102**, 7338 (1998).
[28] See Supplemental Material at http://link.aps.org/supplemental/10.1103/PhysRevB.97.134309 for more details of the phonon wave packet propagation process and the calculation of transmission coefficients.
[29] H. Kato, H. Maris, and S. Tamura, Physica B **219-220**, 696 (1996).
[30] A. G. Every, W. Sachse, K. Y. Kim, and M. O. Thompson, Phys. Rev. Lett. **65**, 1446 (1990).
[31] T. S. Fisher, in *Thermal Energy at the Nanoscale* (World Scientific, Singapore, 2013), pp. 87–111.
[32] T. Zeng and G. Chen, Micros. Thermophys. Eng. **5**, 71 (2001).